Protein dynamics-induced variation of excitation energy transfer pathways

M. Brecht[1], V. Radics, J. B. Nieder, and R. Bittl

Fachbereich Physik, Freie Universität Berlin, Arnimalle 14, 14195 Berlin, Germany

Edited by Nicholas J. Turro, Columbia University, New York, NY, and approved May 26, 2009 (received for review April 2, 2009)

Strong anticorrelation between the fluorescence emission of different emitters is observed by employing single-molecule fluorescence spectroscopy on photosystem I at cryogenic temperatures. This anticorrelation demonstrates a time-dependent interaction between pigments participating in the exciton transfer chain, implying that uniquely defined energy transfer pathways within the complex do not exist. Fluctuations of the chromophores themselves or their immediate protein surroundings induce changes in their site energy, and, as a consequence, these fluctuations change the coupling within the excitation transfer pathways. The time scales of the site energy fluctuations of the individual emitters do not meet the time scales of the observed correlated emission behavior. Therefore, the emitters must be fed individually by energetically higher lying states, causing the observed intensity variations. This phenomenon is shown for photosystem I pigment–protein complexes from 2 different cyanobacteria (*Thermosynechococcus elongatus* and *Synechocystis* sp. PCC 6803) with strongly different spectral properties underlining the general character of the findings. The variability of energy transfer pathways might play a key role in the extreme robustness of light-harvesting systems in general.

exciton transfer | FRET | light harvesting | photosynthesis | single-molecule

The complex structural dynamics of proteins as a result of their combination of properties resembling, in part, the crystalline, the glassy, and the liquid state of matter is a prerequisite for protein function (1, 2). The picture of transitions between hierarchically ordered minima in a multidimensional configuration energy landscape (3) has emerged from the pioneering experiments of Frauenfelder et al. (4) as well as molecular dynamics simulations (5, 6). Local minima correspond to conformational substates (CS) separated by energy barriers into distinct tiers. Protein-embedded chromophore cofactors are ideal reporters for transitions between CS because of the susceptibility of their electronic transition energies on the specific conformation of their protein environment (2). The changes of the electronic transition energies (site energies) of individual chromophores are accessible by single-molecule spectroscopy (SMS) (7) on the single-protein level (8–14).

The transition rates between different CS in proteins are spread out over an extremely wide range of time scales. As a consequence, for room temperature single-molecule experiments on pigment–protein complexes only transitions between CS of higher tiers occurring slower than the presently achievable time resolution of $\approx 0.1\ s^{-1}$ can be monitored directly (14, 15). There, the individual spectra approximately resemble ensemble-averaged spectra with characteristic fluctuations in their width and specific position (13). Lowering the temperature slows down the transitions between CS in high tiers beyond realistic durations of the experiment, and transitions involving lower tiers move into the experimentally accessible time window (11).

SMS experiments on bacterial light-harvesting complex 2 (LH2) and PSI showed that transitions between CS in the lower tiers involve small conformational changes still accessible for the protein at cryogenic temperatures (9, 16). These changes alter the site energies of chlorophyll *a* (Chla) molecules in the nanometer-range. A large portion of the spectral dynamics within the low tiers is connected with exchangeable hydrogens located close to the chromophores, e.g., within hydrogen bonds between the Chla molecules and nearby amino acid residues or structural water molecules (17).

In this study, we focus on PSI (18) of oxygenic photosynthesis from the cyanobacteria *Thermosynechococcus elongatus* and *Synechocystis* sp. PCC 6803. The antenna system consists of ≈90 Chla molecules building a very effective exciton transfer network, which allows efficient excitation of PSI at the maximum of its absorption (≈680 nm) far from the 700-nm absorption of the pigments, P700, responsible for the primary photochemistry in PSI (19, 20). A part of the Chla molecules in the antenna system has site energies <700 nm. These low-energy pigments are often called the "red pools" or the "red-most" chlorophylls [for a review, see Gobets et al. (19), Karapetyan et al. (20), and Brecht (21)].

A very interesting property of PSI is its high quantum yield for charge separation upon exclusive low-energy excitation of its red pool Chlas at ambient temperatures. The energy required for P700 activation is provided by thermal energy. At low temperatures, the reduced thermal energy is insufficient for this process, and the low-energy Chla act as end points of the excitation transfer network. Under these conditions, the excitation energy is partially released as fluorescence light (22) with the maximum of the fluorescence emission found at wavelengths >715 nm. The number and the spectroscopic characteristics of these traps vary remarkably between PSI from different organisms (9, 17, 23–30). The efficient energy transfer from high-energy antenna states to the red pools is very advantageous in SMS because the whole fluorescence emission of PSI can be observed without interference by the excitation light, and the released fluorescence light contains information on the exciton transfer within PSI. Up to now, it is under discussion whether the energy transfer within this antenna system proceeds along well-defined pathways or utilizes variable routes (31).

We address this question with time-resolved fluorescence emission spectroscopy on single PSI complexes. The emission intensity of different pools shows anticorrelated behavior during time. The observation of this anticorrelation for spectroscopically different PSI complexes from 2 species underlines the general character of the findings. The results imply that consideration of static heterogeneities of the transition energies in light-harvesting systems and in macromolecular complexes in general is insufficient. For a proper theoretical description of energy transfer processes, time-dependent fluctuations will have to be taken into account.

Author contributions: M.B. and R.B. designed research; V.R. and J.B.N. performed research; M.B., V.R., J.B.N., and R.B. analyzed data; and M.B. and R.B. wrote the paper.

The authors declare no conflict of interest.

This article is a PNAS Direct Submission.

[1]To whom correspondence should be addressed. E-mail: marc.brecht@physik.fu-berlin.de.

This article contains supporting information online at www.pnas.org/cgi/content/full/0903586106/DCSupplemental.

Results

Emission Properties of PSI from *T. elongatus*. The low-temperature bulk-fluorescence emission spectrum for PSI from *T. elongatus* shows a maximum at ≈730 nm (22). The fluorescence emission consists at minimum of 4 red pools with different spectroscopic properties. They were named C708, C715, C719, and C735 according to their proposed mean absorption wavelength. Two of these pools (C708 and C719) were identified by absorption (22), one by hole-burning spectroscopy (C715) (30) and one by SMS (C735) (25).

The fluorescence emission of single PSI complexes from *T. elongatus* can be separated into 2 wavelength regions, the region <717 nm, where for almost all complexes, wavelength-stable zero-phonon lines (ZPLs) can be observed and the region >717 nm, where the observation of ZPLs is rare (9). The emission in the region between ≈704 and 717 nm dominated by ZPLs can be associated with emission of C708, whereas the emission in region >717 nm is due to emission of C715/719. The orientations of the transition dipole moments of these emitters differ remarkably (22, 25). The low probability of observing ZPLs in the spectral range of C715/719 is due to increased spectral diffusion acting on these chromophores (9, 17). As a consequence, the highly dynamic ZPLs change their position faster than the experimental time resolution and mostly only broad intensity distributions can be observed (9, 17).

Fig. 1*A* shows a series of continuously taken fluorescence emission spectra measured on a single PSI complex from *T. elongatus* at 1.4 K. The average spectrum is shown on top of the sequence. In the average spectrum, a ZPL of C708 at 712 nm can be identified. In the spectral region of C715/719 (>712 nm) an unstructured broad distribution with maximum ≈723 nm is observed. The broad emission band shows, even in spectra taken within 1-s acquisition time, no evidence for ZPLs. The emission intensity of the ZPL and the broad emission undergo large and opposite variations. It is important to note that the broad intensity distribution varies uniformly. For better visualization of these variations, the integrated fluorescence intensities of the ZPL in the wavelength region Λ_1 (from 711.5 to 712.5 nm) and an arbitrary interval of the same width Λ_2 (from 724.5 to 725.5 nm) for the broad intensity distribution are plotted against time (Fig. 1*B*). The intensity variations of the ZPL (Λ_1) and the broad band (Λ_2) are anticorrelated over the whole time of data acquisition. The strong anticorrelation between these 2 traces is reflected by a correlation coefficient $r(\Lambda_1, \Lambda_2) = -0.8$.

Insights into the wavelength dependence of the correlation behavior are given by the 2-dimensional synchronous correlation spectrum [2D-SCS; see supporting information (SI) and ref. 32] as shown in Fig. 1*C*. In the 2D-SCS, autocorrelation and cross-correlation peaks are present. Autopeaks are found at positions of the ZPL and of the broad intensity distribution. The intense autopeak of the ZPL covers a small area in agreement with its narrow line shape in the average spectrum. Accordingly, an extended autopeak is found in the spectral range of the broad intensity distribution. The intensity of this extended autopeak increases from ≈716 to 720 nm, followed by a region with almost constant intensity (720–728 nm) and a smooth decay for $\lambda > 728$ nm.

Cross-peaks indicative for correlation between different spectral components are found between the position of the ZPL and its phonon wing (PW) as well as between the ZPL and the broad intensity distribution. Cross-peaks due to positive correlation of the ZPL with its PW are found in form of 2 narrow extensions of the ZPL autopeak. A narrow ridge represents the negative cross-peak between the ZPL and the broad intensity distribution. This negative cross-peak covers the whole emission range of the ZPL and the broad intensity distribution. Decreasing strength of correlation toward longer wavelength can be associated with decrease of emission intensity (33).

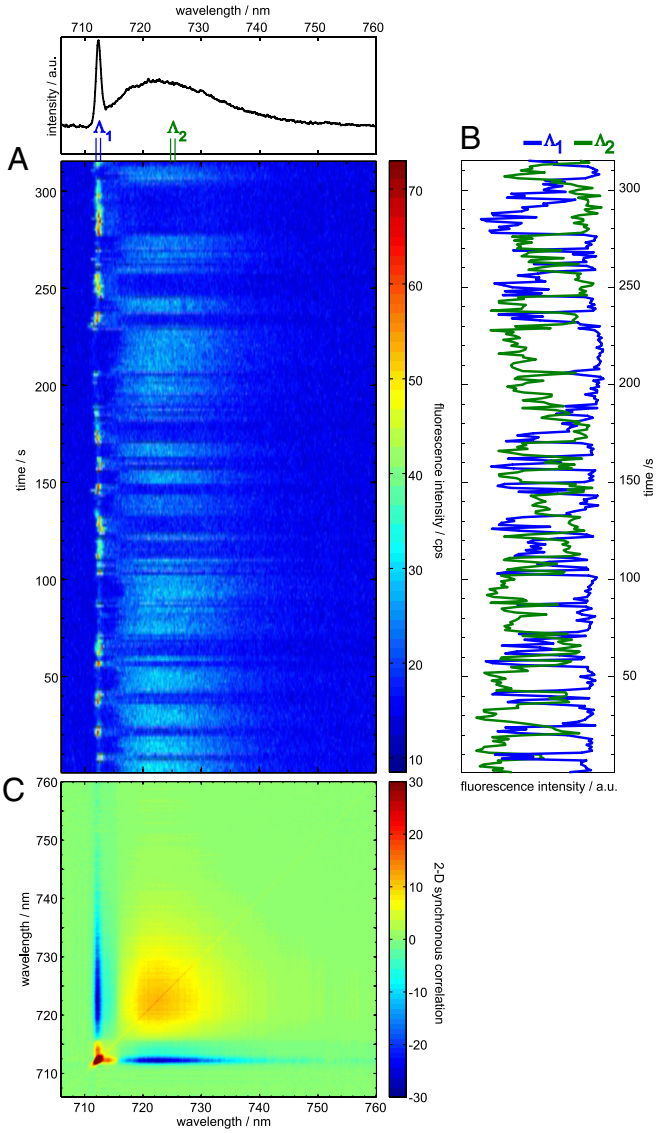

Fig. 1. Time dependent fluorescence emissions from a single PSI complex from *T. elongatus*. (*A*) Time series of spectra; the spectrum on top represents the time average. (*B*) Integrated intensity of the wavelength ranges Λ_1 (712.2–713 nm), and Λ_2 (724.8–725.6 nm). The blue line shows the time dependence of the intensity of the ZPL (Λ_1), and the green line represents the time dependence of a part of the broad emission (Λ_2). (*C*) Contour plot of the 2D-SCS for the sequence given in *A*. The color code is indicated on the right; positive values correspond to positive correlation, and negative values correspond to anticorrelation.

Emission Properties of PSI from *Synechocystis* sp. PCC 6803. The low-temperature bulk-fluorescence emission spectrum of PSI from *Synechocystis* sp. PCC 6803 shows its maximum at ≈718.5 nm (34). The fluorescence emission is made up at minimum by 3 pools called F699, C706, and C714. The pool F699 has its fluorescence emission maximum at 699 nm and was determined by SMS (24). C706 and C714 were proposed based on hole-burning spectroscopy and named according to their absorption maxima (26–28, 30). The fluorescence emission maxima for C706 and C714 are expected at ≈710 and ≈720 nm, respectively (26). The effect of spectral diffusion differs for these 3 contributions (17, 24). F699 shows the least effect; therefore, stable

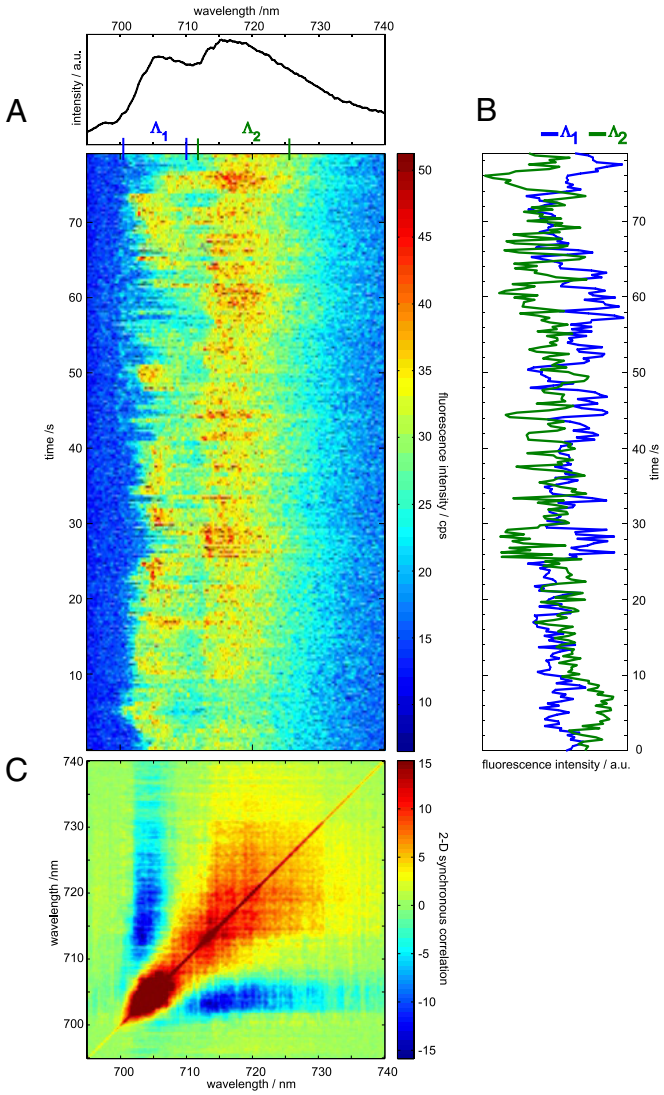

Fig. 2. Time dependent fluorescence emission from a single PSI complex from *Synechocystis* sp. PCC 6803. (*A*) Time series of spectra; the spectrum on top represents the time average. (*B*) Integrated intensity of the wavelength ranges Λ_1 (700.5–710 nm) and Λ_2 (712–725.5 nm). The blue line shows the time dependence of the intensity of the ZPL (Λ_1) and the green line represents the time dependence of a part of the broad emission (Λ_2). (*C*) Contour plot of the 2D-SCS for the sequence given in *A*. The color code is indicated on the right; positive values correspond to positive correlation, and negative values correspond to anticorrelation.

ZPLs dominate the fluorescence emission at the single-molecule level. For C706 and C714, the impact of spectral diffusion is larger. C706 shows stable ZPLs in one-third of the investigated complexes, and for C714 observation of ZPLs remains an exception (24).

Fig. 2*A* shows a series of continuously taken fluorescence emission spectra measured on a single PSI complex from *Synechocystis* sp. PCC 6803 at 1.4 K. The average spectrum is shown on top of the sequence.

The average spectrum shows 2 broad maxima at ≈706 and ≈717 nm. These broad contributions are most likely due to the emitters C706 and C714, respectively. In the time sequence, no evidence for stably emitting ZPLs is found, therefore both contributions are subject to fast spectral diffusion (24). The time-dependent variations of the emission frequency and intensity suggest a single emitter as origin of these contributions. For better visualization of these intensity variations, the fluorescence intensities in the range of 700–710 nm (Λ_1) and 713–726 nm (Λ_2) are displayed in Fig. 2*B*. These time traces show clear anticorrelation with a correlation coefficient $r(\Lambda_1, \Lambda_2) = -0.4$.

The corresponding 2D-SCS of the sequence is given in Fig. 2*C*. Autopeaks and cross-peaks are found for the emitters centered at 706 nm and 717 nm. The extension of the autopeaks is in agreement with the line shape in the average spectrum. A large negative cross-peak covers almost the whole emission region of the 2 emitters, indicating strong anticorrelation between the contributions from C706 and C714.

Discussion

Two possibilities for an interpretation of the observed anticorrelated red-pool emission in PSI are apparent. The first involves an extension of the spectral diffusion argument put forward for explaining the broad single-molecule emission from C719 and C714 pools in *T. elongatus* and *Synechocystis* sp. PCC 6803, respectively. There, a variability of the emission wavelength of an individual state in the range of 10 nm was invoked (8, 23) and corroborated by observation (17). Assuming an even larger susceptibility of the emission wavelength of an individual emitting state to changes in the environment leads to the hypothesis that the emissions in the range C708 and C719 (C706 and C714) for PSI from *T. elongatus* (*Synechocystis* sp. PCC 6803) arise from only 1 emitting state with time-dependent drastically different realizations of the site energy. However, several independent observations exist, each arguing against the assignment of C708 and C719 (C706 and C714) to 1 chromophore or chromophore assembly. The polarization of C708 and C719 was found to differ substantially, as well in bulk (22, 34) as in single-molecule (24, 25) experiments. This shows drastically different orientations of the transition dipole moments for the emission from C708 and C719. Such a change in the dipole moment is unlikely for 1 emitting state. Second, hole-burning spectroscopy revealed different electron–phonon coupling between the C708 and C719 (C706 and C715) pools (27, 28, 30), suggesting different emitters as the origin of the respective pools. Furthermore, very different spectral diffusion characteristics were found for the 2 emission ranges C708 and C719 in single-molecule experiments (9). This again can hardly be reconciled with 1 emitting state as source for both spectral regions. Therefore, we consider a switching between 2 spectrally distinct realizations of 1 emitting state as very unlikely being the origin of the anticorrelated emission in the ranges C708 and C719 in *T. elongatus* and C706 and C714 in *Synechocystis* sp. PCC 6803.

The second interpretation is based on changes in the excitation energy transfer, and we briefly discuss the model used to describe the excitation energy transport between chromophores. This is usually done within the framework of FRET originally developed by Förster (35). In this model, 2 main contributions control the transfer rate (*i*) the excitonic coupling and (*ii*) the spectral overlap of the chromophores. The excitonic coupling is usually calculated within the point dipole approximation. This approximation requires a much larger distance between the chromophores than their own spatial extension. For dense multichromophore assemblies such as PSI, this condition is violated, and more detailed calculation of the coupling is necessary for a quantitative understanding of transfer rates (36). Further complications arise from the fact that the excitation energies for individual pigments are not fixed. This leads to significant heterogeneity of calculated spectra for different choices of the site energies as it was shown for LH2 (37). In ensemble spectra, the average of these different spectra is observed, whereas in SMS, this heterogeneity can be observed as different behavior of individual complexes. Irrespective of these complications in dense multichromophore systems, the excitonic

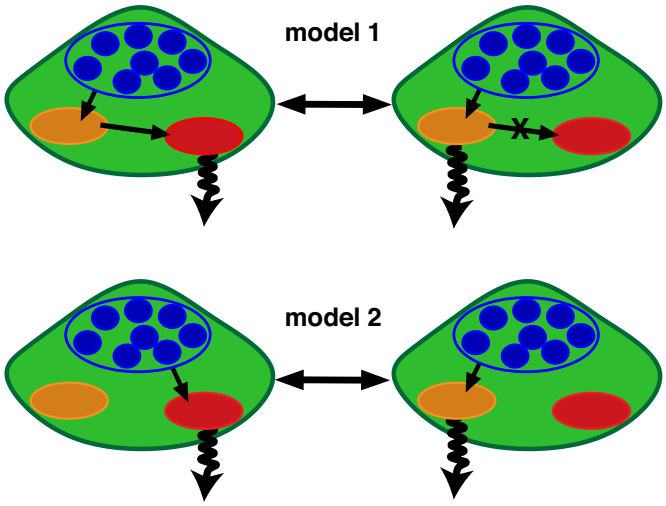

Fig. 3. Schematic representation of 2 simple models for the exciton transfer in PSI. The number of the participating Chla molecules were reduced to the minimal number sufficient for the qualitative description of the observed anticorrelation of the emission intensities given in Fig. 1; those are C708, C715/C719, and main antenna states (*T. elongatus*), the appropriate quantities for *Synechocystis* sp. PCC 6803 are C706, C714, and main antenna states. Model1 illustrates a linear downhill EET from antenna states through the C708 pool into the C715/C719. Model2 illustrates a direct feeding of the pools C708 and C715/C719 by energetically higher lying antenna states.

coupling and spectral overlap determining the FRET rates are adequate for a qualitative interpretation of our results.

In the point dipole approximation, the coupling depends on the inverse of the third power of the distance between the chromophores and on the angle between the transition dipole moments of donor and acceptor. Neither of these geometric parameters has sufficient freedom for significant changes in a protein at low temperatures. The remaining quantity entering the transfer rate is the spectral overlap.

If static site energies are assumed, the different traps are fed with time-independent rates. Under these circumstances, anticorrelation is observed only on the single-photon level. This holds even for a large multichromophore FRET assembly like PSI as long as the multistep energy transfer processes from the main antenna toward the emitting states is substantially faster than the fluorescence lifetime. Averaging over longer times will destroy this initial anticorrelation quickly. Thus, the observed correlated intensity variations on the second timescale involving the emission of $\approx 10^4$ to 10^6 photons cannot be explained with static rates. However, results from time-resolved low-temperature single-molecule spectroscopy showing strong frequency variations of ZPLs provide a basis for understanding our observation. The spectral dynamics of ZPLs reports changes in the site energy of the chromophores (9, 38, 39). The energy transfer rate depends strongly on the spectral overlap of donor and acceptor. This dependence results in a modulation of the energy transfer rates by changes of the site energies (40–42). Based on changes of the relative emission intensity observed in donor/acceptor dyads, it was recently supposed that the spectral overlap between chromophores can vary remarkably even at 1.4 K (43).

Under the assumption of different chromophores as origin of fluorescence emission from PSI in the different spectral regions (see above), the observed anticorrelated emission (Figs. 1 and 2) can be described by 2 simple models for the excitation energy transfer given in Fig. 3. Model 1 assumes a linear downhill energy transfer of the excitation energy from the antenna (blue) to the final trap (red). The anticorrelation is induced by changes in the transfer rates between the 2 red traps (orange, red). Model 2 assumes a parallel feeding of the red traps by energetically higher lying antenna states in the transfer pathway of the exciton. To distinguish between these 2 models, further analysis is needed.

First the dynamic properties of the observable emitters are inspected as potential origin of the observed correlated behavior. The anticorrelated intensity variations (shown in Figs. 1 and 2) occur on a second time scale. In the spectra taken for PSI from *T. elongatus*, the emitter C708 undergoes virtually no change of its emission frequency, whereas the spectral dynamics of C715/C719 is much faster than the required second time scale. Therefore, both pools have to be excluded as source for the observed intensity variations. The same holds for *Synechocystis* sp. PCC 6803 (Fig. 2) where both emitters show spectral dynamics much faster than the second time-scale of the intensity anti-correlation.

As a consequence, direct transfer of the exciton energy (model 1) from C708 (*T. elongatus*)/C706 (*Synechocystis* sp. PCC 6803) to C719 (*T. elongatus*)/C714 (*Synechocystis* sp. PCC 6803) has to be excluded at least for the fraction of the emission intensity of C719/C714 being anti-correlated to the intensity of C708/C706 (model 1, Fig. 3). Therefore, we conclude, the anticorrelated intensity behavior must be induced by energetically higher lying states within the antenna system (model 2). The anticorrelation observed in the emission is induced by spectral dynamics of these states happening on a second time scale according to the observed intensity variations. This dynamics is independent of the spectral dynamics of the red pool emitters. The excitation energy is fed into different pathways with individual energetic traps depending on the actual site energy of the energetically higher lying states, and the final traps are not connected by efficient direct excitation energy transfer (EET) between each other.

The variation of the EET at low temperatures has a direct consequence for the discussion of EET in PSI at ambient conditions. Although all models for the EET analyzed so far assumed, at best, a static distribution of site energies, it seems much more appropriate to include also fluctuations of the site energies for realistic modeling of EET in PSI and similar complexes.

At ambient temperatures, many more degrees of freedom are available for conformational changes of the protein, and thus the coupling between the protein and the cofactor leads to a faster modulation of the site energies, probably on the subnanosecond time scale. This time scale is much shorter than the average time between 2 photon absorption events in 1 PSI complex under ambient light conditions. Therefore, the changes in site energies between 2 successive absorption events likely lead to different EET pathways for each exciton. The variability of the EET pathways induced by protein dynamics might play a key role in the high photostability of PSI and might give a hint to the robustness of proteins in general. Furthermore, our finding shows that tiny changes in the 3-dimensional structure of the complex are able to vary the excitation transfer pathway in PSI remarkably. At low temperature, the observed spectral dynamics is, at least partially, photoactivated (11, 38, 39). Under strong illumination at ambient conditions, such photoactivated dynamics can increase the rate of fluctuations in the EET pathway or even alter the preferential EET route away from the reaction center toward protective quenching sites. The finding of protein dynamics induced alterations of EET pathways points toward an efficient protection mechanism.

Materials and Methods

PSI from the *T. elongatus* and *Synechocystis* sp. PCC 6803 were prepared as described (9, 24). Less than 1 μL of the sample was placed between 2 coverslips, assuring spatial separation of individual PSI trimers. Sample preparation and mounting were accomplished under indirect daylight.

We used a home-built confocal microscope to observe the fluorescence emission of single PSI complexes. The experimental setup was described in more detail recently in ref. 9. The sample and the microscope objective were immersed in superfluid He, and the sample temperature was 1.4 K during all experiments. Excitation wavelength was 680 nm, and the power measured directly behind the beam-scanning module was 100 μW for all spectra. At 1.4 K, we reach almost the low temperature limit, where the shape of a single emitting species in the condensed phase consists of a narrow ZPL and a broad phonon wing (PW) (44). The ZPL belongs to an electronic transition without phonon (lattice vibrational modes) creation or annihilation. The PW on the low-energy side of the ZPL is due to the interaction of the chromophore with its surrounding leading to the excitation of phonons.

ACKNOWLEDGMENTS. We thank Eberhard Schlodder for providing the samples and helpful discussion, Andreas Modler, and Hauke Studier for helpful discussion. We are grateful to a reviewer for a valuable comment. In addition, we acknowledge support from the Cluster of Excellence ''Unifying Concepts in Catalysis'' funded by the Deutsche Forschungsgemeinschaft.

1. Frauenfelder H, Slia SG, Wolynes PG (1991) The energy landscapes and motions of proteins. *Science* 254:1598–1603.
2. Lindorff-Larsen K, Best RB, DePristo MA, Dobson CM, Vendruscolo M (2005) Simultaneous determination of protein structure and dynamics. *Nature* 433:128–132.
3. Miyashita O, Onuchic JN, Wolynes PG (2003) Nonlinear elasticity, proteinquakes, and the energy landscapes of functional transitions in proteins. *Proc Natl Acad Sci USA* 100:12570–12575.
4. Fraunenfelder H, Petsko GA, Tsernoglou D (1979) Temperature-dependent X-ray-diffraction as a probe of protein structural dynamics. *Nature* 280:558–563.
5. Elber R, Karplus M (1987) Multiple conformational states of proteins—A molecular-dynamics analysis of myoglobin. *Science* 235:318–321.
6. van Gunsteren, et al. (2006) Biomolecular modeling: Goals, problems, perspectives. *Angew Chem Int Ed* 45:4064–4092.
7. Tamarat P, Maali A, Lounis B, Orrit M (2000) Ten years of single-molecule spectroscopy. *J Phys Chem A* 104:1–16.
8. Jelezko F, Tietz C, Gerken U, Wrachtrup J, Bittl R (2000) Single-molecule spectroscopy on photosystem I pigment–protein complexes. *J Phys Chem B* 104:8093–8096.
9. Brecht M, Studier H, Elli AF, Jelezko F, Bittl R (2007) Assignment of red antenna states in photosystem I from *Thermosynechoccocus elongatus* by single-molecule spectroscopy. *Biochemistry* 46:799–806.
10. Edman L, Rigler R (2000) Memory landscapes of single-enzyme molecules. *Proc Natl Acad Sci USA* 97:8266–8271.
11. Hofmann C, et al. (2003) Single-molecule study of the electronic couplings in a circular array of molecules: Light-harvesting-2 complex from *Rhodospirillum molischianum*. *Phys Rev Lett* 90:013004.
12. Kiraz A, Ehrl M, Bräuchle C, Zumbusch A (2003) Low temperature single molecule spectroscopy using vibronic excitation and dispersed fluorescence detection. *J Chem Phys* 118:10821–10824.
13. Rutkauskas D, Novoderezhkin V, Cogdell RJ, van Grondelle R (2005) Fluorescence spectroscopy of conformational changes of single LH2 complexes. *Biophys J* 88:422–435.
14. Rutkauskas D, Novoderezkhin V, Cogdell RJ, van Grondelle R (2004) Fluorescence spectral fluctuations of single LH2 complexes from *Rhodopseudomonas acidophila* strain 10050. *Biochemistry* 43:4431–4438.
15. Lu HP, Xie XS (1997) Single-molecule spectral fluctuations at room temperature. *Nature* 385:143–146.
16. Hofmann C, Aartsma TJ, Michel H, Kohler J (2003) Direct observation of tiers in the energy landscape of a chromoprotein: A single-molecule study. *Proc Natl Acad Sci USA* 100:15534–15538.
17. Brecht M, Studier H, Radics V, Nieder JB, Bittl R (2008) Spectral diffusion induced by proton dynamics in pigment–protein complexes. *J Am Chem Soc* 130:17487–17493.
18. Jordan P, et al. (2001) Three-dimensional structure of cyanobacterial photosystem I at 2.5-Angstrom resolution. *Nature* 411:909–917.
19. Gobets B, van Grondelle R (2001) Energy transfer and trapping in photosystem I. *Biochim Biophys Acta Bioenerg* 1507:80–99.
20. Karapetyan NV, Schlodder E, van Grondelle R, Dekker JP (2007) in *Advances in Photosynthesis and Respiration. Photosystem I: The Light-Driven Plastocyanin:Ferredoxin Oxidoreductase*, ed Golbeck JH (Springer, Berlin), Vol 24.
21. Brecht M (2009) Spectroscopic characterization of photosystem I at the single-molecule level. *Mol Phys* 10.1080/00268970902859777.
22. Palsson LO, Dekker JP, Schlodder E, Monshouwer R, van Grondelle R (1996) Polarized site-selective fluorescence spectroscopy of the long-wavelength emitting chlorophylls in isolated Photosystem I particles of *Synechococcus elongatus*. *Photosynth Res* 48:239–246.
23. Brecht M, Nieder JB, Studier H, Schlodder E, Bittl R (2008) Red antenna states of photosystem I from *Synechococcus* sp. PCC 7002. *Photosynth Res* 95:155–162.
24. Brecht M, Radics V, Nieder JB, Studier H, Bittl R (2008) Red antenna states of photosystem I from *Synechocystis* PCC 6803. *Biochemistry* 47:5536–5543.
25. Elli AF, et al. (2006) Red pool chlorophylls of photosystem I of the cyanobacterium *Thermosynechococcus elongatus*: A single-molecule study. *Biochemistry* 45:1454–1458.
26. Hayes JM, Matsuzaki S, Ratsep M, Small GJ (2000) Red chlorophyll a antenna states of photosystem I of the cyanobacterium *Synechocystis* sp PCC 6803. *J Phys Chem B* 104:5625–5633.
27. Hsin TM, Zazubovich V, Hayes JM, Small GJ (2004) Red antenna states of PSI of cyanobacteria: Stark effect and interstate energy transfer. *J Phys Chem B* 108:10515–10521.
28. Ratsep M, Johnson TW, Chitnis PR, Small GJ (2000) The red-absorbing chlorophyll *a* antenna states of photosystem I: A hole-burning study of *Synechocystis* sp PCC 6803 and its mutants. *J Phys Chem B* 104:836–847.
29. Riley KJ, Reinot T, Jankowiak R, Fromme P, Zazubovich V (2007) Red antenna states of photosystem I from cyanobacteria *Synechocystis* PCC 6803 and *Thermosynechococcus elongatus*: Single-complex spectroscopy and spectral hole-burning study. *J Phys Chem B* 111:286–292.
30. Zazubovich V, et al. (2002) Red antenna states of photosystem I from cyanobacterium *Synechococcus elongatus*: A spectral hole burning study. *Chem Phys* 275:47–59.
31. Byrdin M, et al. (2002) Light harvesting in photosystem I: Modeling based on the 2.5-Angstrom structure of photosystem I from *Synechococcus elongatus. Biophys J* 83:433–457.
32. Noda I, Dowrey AE, Marcott C, Story GM, Ozaki Y (2000) Generalized two-dimensional correlation spectroscopy. *Appl Spectrosc* 54:236A–248A.
33. Yu ZW, Liu J, Noda I (2003) Effect of noise on the evaluation of correlation coefficients in two-dimensional correlation spectroscopy. *Appl Spectrosc* 57:1605–1609.
34. Gobets B, et al. (1994) Polarized site-selected fluorescence spectroscopy of isolated photosystem-I particles. *Biochim Biophys Acta Bioenerg* 1188:75–85.
35. Forster T (1946) Das Fluoreszenzvermögen organischer Farbstoffe. *Naturwissenschaften* 33:166–175.
36. Scholes GD, Jordanides XJ, Fleming GR (2001) Adapting the Förster theory of energy transfer for modeling dynamics in aggregated molecular assemblies. *J Phys Chem B* 105:1640–1651.
37. Fleming GR, Scholes GD (2004) Physical chemistry—Quantum mechanics for plants. *Nature* 431:256–257.
38. Hofmann C, Michel H, van Heel M, Kohler J (2005) Multivariate analysis of single-molecule spectra: Surpassing spectral diffusion. *Phys Rev Lett* 94:195501.
39. Ketelaars M, et al. (2006) Probing the electronic structure and conformational flexibility of individual light-harvesting 3 complexes by optical single-molecule spectroscopy. *J Phys Chem B* 110:18710–18717.
40. Metivier R, et al. (2004) Single-molecule spectroscopy of molecular aggregates at low temperature. *J Lumin* 110:217–224.
41. Becker K, et al. (2006) Electrical control of Förster energy transfer. *Nat Mater* 5:777–781.
42. Metivier R, Nolde F, Mullen K, Basche T (2007) Electronic excitation energy transfer between two single molecules embedded in a polymer host. *Phys Rev Lett* 98:047802.
43. Hinze G, Metivier R, Nolde F, Mullen K, Basche T (2008) Intramolecular electronic excitation energy transfer in donor/acceptor dyads studied by time and frequency resolved single molecule spectroscopy. *J Chem Phys* 128:124516.
44. Jankowiak R, Hayes JM, Small GJ (1993) Spectral hole-burning spectroscopy in amorphous molecular-solids and proteins. *Chem Rev* 93:1471–1502.